CORA Cork Open Research Archive
Cartlann Taighde Oscailte Chorcaí

Title	Core-shell nanoarchitectures for lithium-ion energy storage applications
Authors	Clancy, Tomás M.;Rohan, James F.
Publication date	2016-03-22
Original Citation	Clancy, T. M. and Rohan, J. F. (2016) 'Core-shell nanoarchitectures for lithium-ion energy storage applications', MRS Advances, 1(15), pp. 1055-1060. doi:10.1557/adv.2016.216
Type of publication	Article (peer-reviewed)
Link to publisher's version	10.1557/adv.2016.216
Rights	© 2016, Materials Research Society. Published by Cambridge University Press. This article has been published in a revised form in MRS Advances [https://doi.org/10.1557/adv.2016.216]. This version is free to view and download for private research and study only. Not for re-distribution, re-sale or use in derivative works.
Download date	2026-11-04 07:07:07
Item downloaded from	https://hdl.handle.net/10468/6490



UCC
University College Cork, Ireland
Coláiste na hOllscoile Corcaigh

Core-shell Nanoarchitectures for Lithium-Ion Energy Storage Applications

Tomas M. Clancy[1] and James F. Rohan[1]
[1]Tyndall National Institute, University College Cork, Lee Maltings, Cork, Ireland

ABSTRACT

Multiphysics simulations (COMSOL) of core-shell nanoarchitectures show that they can operate at 3 times the C-rate of micron scale thin film materials while still accessing 90% of an additive free cathode oxide material. A high performance Ge anode DC sputtered onto a Cu nanotube current collector is characterised. Volume expansion of Ge is alleviated and mechanical stability is enhanced due to the Cu nanotubes current collector.

INTRODUCTION

As the device dimensions decrease, and more functionality is added or devices become more autonomous, energy provision and storage become prominent issues for integrated energy storage on chip. Lithium-ion batteries are the leading contender for integration with microelectronic devices having a high gravimetric and volumetric capacity and also being a mature technology. Thin-film solid state batteries processed on silicon substrates with excellent cycle life are being developed for such devices. Low conductivity and slow transport of ions in the solid state materials means the additive free cathode thickness is limited to micrometers (<5μm) in a 2D geometry therefore limiting the energy storage per area. Nanoarchitectures and higher specific energy electrode materials need to be developed for lithium-ion batteries to meet the increased energy and power density demand.

The electrochemical reaction and ion transport in a lithium battery is influenced by the geometry and size of the electrodes. 3D architectures allow for more electrode surface area to be in direct contact with the electrolyte and theoretically increase the power density. Mathematical models first developed by Newman et al. have been used to describe the electrochemical reactions in 2D and 1D porous lithium-ion batteries [1]. Recent multiphysics simulations have used these mathematical models and applied them to 3D nanoarchitectures to gain an understanding of the electrochemical reactions [2].

High capacity anode materials such as Si (theoretical capacity 4200 mAh/g) and Ge (1623 mAh/g) both undergo a volume expansion of up to 300% which results in low cycle life in its bulk state due to delamination and structural disintegration from the current collector. 3D nanoarchitectures have been shown to alleviate the effect of volume expansion, enhancing mechanical stability at the nanoscale [3]. Ge has many advantages over Si as an anode material for high power applications with 400 times higher rate of Li^+ diffusion at room temperature and 10,000 times the electrical conductivity [4, 5]. Reported 3D geometries of Ge electrodes to date have been nanowires [6], nanotubes [7] and direct deposition onto the 3D current collector [8].

In this work, multiphysics simulations based on COMSOL modules have been used to compare relatively low conductive cathode oxide materials in solid state thin-film micro, nanowire and core-shell nanowire battery geometries. Improved performance Ge electrodes as a

high capacity anode material for lithium-ion batteries is also demonstrated. The method used DC sputtering of Ge layers onto a Cu nanotube array that acted as a current collector.

EXPERIMENTAL

COMSOL lithium-ion battery and transport of diluted species modules were used to model the thin-film solid state lithium-ion battery. These modules use predefined mathematical equations and assumptions [1]. The battery materials simulated were $LiCoO_2$ cathode, Li metal anode and a 1M $LiPF_6$ in solvent electrolyte. Non-porous electrodes were used so that only Li^+ ion transportation through the electrode/electrolyte boundary areas is considered.

All three geometries had an out of plane thickness of 100 µm and volume of $2.5x10^{-16}$ m^3. The microbattery thin film geometry comprised 5 µm thick electrodes separated by 2 µm of electrolyte. The nanowire battery geometry was composed of nanowire electrodes with a height of 5 µm and diameter of 500 nm, cathode and anode nanowire electrodes were separated by 2 µm and have a spacing of 350 nm filled with electrolyte. The core-shell nanowire geometry was 200 nm diameter conductive nanowire current collector with a height of 4.72 µm that was covered with active electrode material. The core-shell nanowire electrodes had an overall height and diameter of 4.92 µm and 700 nm respectively. The cathode and anode electrodes were separated by 2 µm and a spacing of 350 nm filled with electrolyte.

Table I. Parameters used in COMSOL multiphysics simulations.

Symbol	Description	Value
c_{Li_init}	Initial Li^+ concentration in electrolyte	1000 mol m^{-3}
c_{init}	Initial Li^+ concentration in cathode	24400 mol m^{-3}
c_{max}	Maximum Li^+ concentration in cathode	51600 mol m^{-3}
D	Diffusion coefficient for Li^+ in cathode	$5x10^{-13}$ m^2 s^{-1}
D_{Li}	Diffusion coefficient for Li^+ in electrolyte	$7x10^{-11}$ m^2 s^{-1}
$conduct_{pos}$	Conductivity of cathode	$1x10^{-6}$ S cm^{-1}
$conduct_{neg}$	Conductivity of anode	$1.05x10^{5}$ S cm^{-1}
$conduct_{electroylte}$	Conductivity of electrolyte	$1x10^{-6}$ S cm^{-1}
k_{pos}	Rate constant charge transfer of cathode	$1.27x10^{-6}$ A m^{-2} (mol m^{-3})$^{-1.5}$
i_{0_neg}	Exchange current density of anode	85 A m^{-2}
t_o	Transference number	0.5
α	Transfer coefficient	0.5
T	Temperature	298.15

For this study an extremely fine edge mesh was used on the electrode/electrolyte boundaries while the mesh for the remaining geometry was extra fine free triangular mesh. A parametric sweep was used to vary the discharge C-rate. The time dependent study was between 0 and 3600 s with a relative tolerance of 1e-4. The stop condition was time step <1e-10.

The design and fabrication of the Cu nanotube core/Ge shell anode is shown in figure 1. Cu nanotubes were fabricated as described earlier [9].

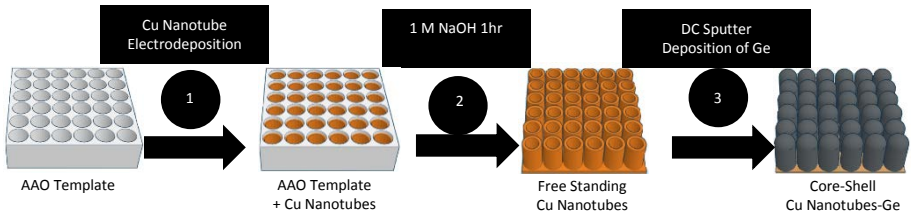


Figure 1. Schematic of the design and fabrication of Cu nanotube core/Ge shell anode. (1) Cu nanotube electrodeposition; (2) AAO template dissolved in 1 M NaOH; (3) DC sputtering of Ge onto the surface of the Cu nanotubes.

Ge was deposited onto the surface of the Cu nanotube array using a 99.99% pure Ge target (Kurt J. Lesker) and was DC-sputtered (Quorum Q300T D Dual) at a pressure of $1x10^{-2}$ mBar. The sputtering current used was 90 mA for 6, 12 and 24 min.

The structure and the morphology of the samples were analysed (FEI Nova 630 Nano-SEM) coupled with an energy dispersive X-ray (EDX) (Hitachi S4000), X-ray powder diffraction (XRD) (Philips PW3710-MPD with Cu Kα radiation, $\lambda = 1.54056$ Å, at 45 kV (40 mA), and data was analysed using Philips X'Pert XRD software), Raman spectroscopy (Renishaw Invia, 514 nm laser) and four point probe analysis (Agilent 34401A multimeter and Wayne Kerr Electronics, LS30-10 power supply) were performed. Electrochemical measurements of the Li^+ capacity were assessed by cyclic voltammetry (CV) and galvanostatic intermittent titration technique (GITT) using a potentiostat (Bio-logic VSP) at various scan rates and discharge/charge currents, respectively. A two electrode cell setup of lithium foil 0.25 mm thick (Sigma Aldrich) acted as counter and reference and the Cu nanotube core/Ge shell anode as the working electrode in 1 M $LiPF_6$ in ethylene carbonate/diethyl carbonate (50:50 volume) (Sigma Aldrich) electrolyte assembled in an argon-filled glove box (M. Braun LABstar Glove Box) with O_2 and H_2O maintained below 0.1 ppm.

DISCUSSION

Concentration profiles and discharge curves were used to evaluate the electrochemical activity of the COMSOL simulations of the battery geometries with a cut-off potential of 2.5 V. The diffusion coefficient and conductivity value used are based on an optimum LiPON solid state electrolyte. The $LiCoO_2$ simulated without any conductive additives had a low conductivity value of $1x10^{-6}$ S cm^{-1} which is 3 orders of magnitude lower than $LiCoO_2$ with conductive additives. The concentration profiles in figure 2a show that Li distribution has the best uniformity in the core-shell nanowire geometry and the nanowire geometry with the thin film geometry being the least uniform. The thin film geometry shows that the bulk of the Li concentration is at the electrode/electrolyte interface and with very little Li at the base of the electrode. The core-shell nanowire and nanowire geometry have better Li uniformity due to more electrode surface area exposed to the electrolyte. Figure 2b shows the simulated battery discharge capacity at specific C-rates for the thin-film, nanowire and core-shell nanowire geometries. The internal resistance from the low conductivity of the $LiCoO_2$ and electrolyte for the planar thin-film version leads to rapid decrease in performance (less capacity utilized) above 7C. At the high discharge rates a large voltage drop forces the potential to go below the practical lower potential limit of 2.5 V.

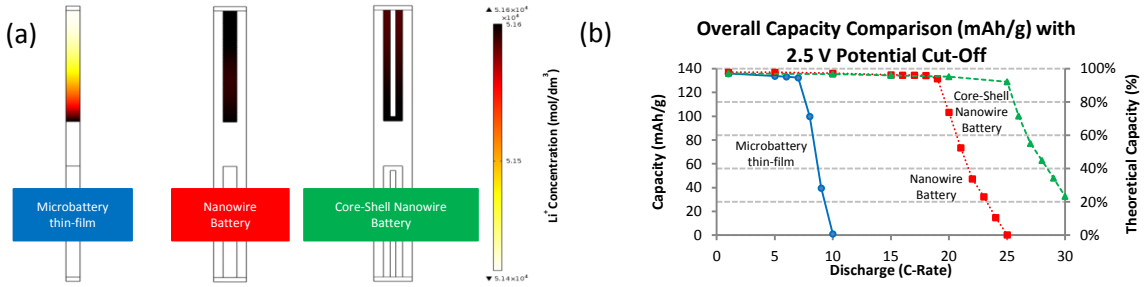


Figure 2. (a) Li concentration profile in cathode for microbattery thin-film, nanowire battery and core-shell nanowire battery at a 1C discharge rate; (b) Overall capacity comparison at various discharge rates.

The simulations suggest the implementation of nanoarchitectures such as nanowires and core-shell nanowires for all solid state batteries could increase the discharge rate up to 16C and 25C respectively with a maximum discharge of the cell capacity 0.11 mAh/cm^2 (or 90% + of the theoretical capacity).

Figure 3a is a SEM and EDX image of the electrodeposited Cu nanotubes current collector. The image shows electrodeposited hollow Cu nanotubes, perpendicular to the Ag seed layer.

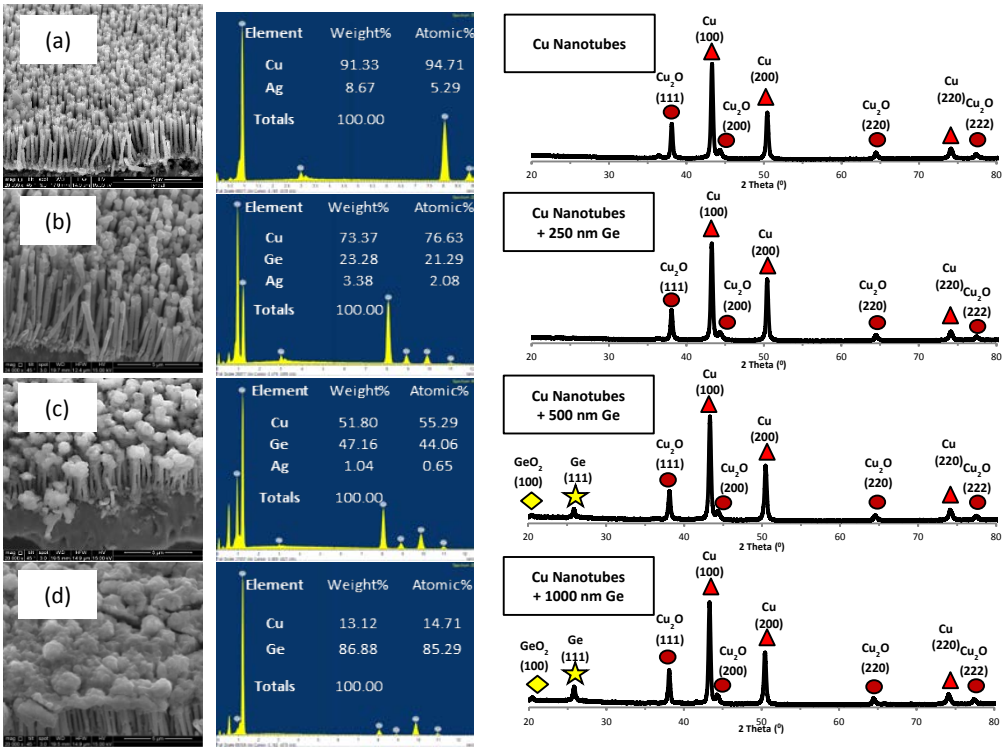


Figure 3. SEM/EDX/XRD of (a) Cu nanotubes; (b) 6 min Ge deposition; (c) 12 min Ge deposition; (d) 24 min Ge deposition.

The SEM and EDX image of the Cu nanotubes with 6, 12 and 24 min (~250 nm, 500 nm and 1000 nm Ge planar deposit respectively) DC sputtered Ge is shown in figure 3b,c,d respectively. The EDX confirms the presence of Ge and Cu as the prevalent elements while the SEM illustrates the deposition of Ge on the Cu nanotubes. Thicker Ge deposits at the top of the Cu nanotubes which eventually forms a thin layer for the longest deposit of 1000 nm. This is due to

the nanoscale spacing between the pores in AAO templates. A larger spacing would give a more uniform deposit. Four point probe conductivity measurements gave a value of $1x10^{-2}$ S cm^{-1} for this undoped Ge. This is in the same order of magnitude as bulk Ge ~$x10^{-2}$ S cm^{-1} and one order of magnitude higher than Ge nanowires reported in the literature [10].

The XRD analysis shown in figure 3a suggests a thin oxide layer exists on the Cu nanotubes. The (111) Ge phase is at 26^0 and the natural oxide GeO_2 phase (100) at 20.50 are present for the 500 nm and 1000 nm deposition in figure 3c,d. The (111) Ge phase is typically found at 27^0 in the literature meaning there is a peak shift of 1^0 suggesting a stress on the lattice structure which is expected for thin films [11,12]. There are no Ge and GeO_2 peaks seen for the 250 nm deposition which is due to the penetration depth of the XRD and the small quantity of Ge deposited. Raman spectroscopy exhibits a single peak at 289.8 cm^{-1} attributed to the Raman active first order transverse optical phonon mode of Ge [13], this is slightly lower than the bulk Ge Raman peak quoted in the literature [14].

The chemical diffusion coefficient of Li in Ge was estimated using GITT with a 0.1C pulse for 10 min followed by a rest period of 10 min. The diffusion coefficient at low lithium concentrations was $2x10^{-10}$ cm^2 s^{-1} and $8x10^{-12}$ cm^2 s^{-1} at high lithium concentrations. This is in agreement with the literature values of $1.5x10^{-10}$ cm^2 s^{-1} and $5x10^{-12}$ cm^2 s^{-1} reported for low and high concentration of lithium respectively [15]. The electrochemical comparison of 250 nm, 500 nm and 1000 nm Ge depositions on the Cu nanotubes was studied by CV and galvanostatic cycling. Figure 4a shows data for cycles 41-45 at a scan rate 0.05 mV/s.

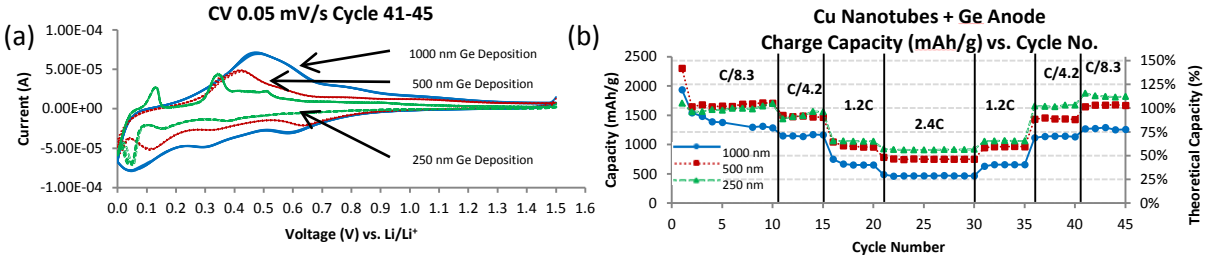


Figure 4. (a) CV cycles 41-45 at a scan speed of 0.05 mV/s for various amounts of Ge sputtered on Cu nanotubes (b) Ge deposit comparison of charge capacity vs. cycle number.

The cathodic peaks at 0.6 V, 0.3 V and 0.05V for the 1000 nm Ge deposition are associated with the formation of the Li-Ge alloy while the broad anodic peak at 0.48 V is associated to the de-alloying of LixGe to Ge. The cathodic peaks increase with deceasing Ge deposition thickness which is expected due to the compressive stress levels into the films [15]. The broad anodic peak at 0.48 V begins so split into two peaks at the 500 nm Ge deposition and is fully split at the 250 nm Ge deposition which is also associated with thin films of Ge. An additional cathodic and anodic peak appears at 0.047 V and 0.13 V respectively for the 250 nm Ge deposition. These peaks are due to the thin Ge deposit and the slow scan speed permitting access the Ge sites hosting Li^+ ions. The CVs of cycles 41-45 show excellent overlap which indicates little or no degradation in performance. The charge capacities for a range of CVs at different scan speeds vs cycle numbers 1-45 is seen in figure 4b, the large initial charge capacity seen during the first cycles are linked to the formation of the SEI layer due to the native oxide of GeO_2 identified from the XRD. Figure 5b highlights the robustness and advantages associated with the 3D core-shell nanoarchitecture as the design allows the Ge to expand and contract without detaching from the Cu nanotube current collector. This permits the Ge anode to have a much longer cycle life with little or no decline in capacity.

CONCLUSIONS

In summary, COMSOL multiphysics simulations have shown better Li^+ ion distribution within the electrode and improved rate capabilities for nanowire and core-shell nanowire battery geometries by comparison with planar micron scale thin film micro-batteries. These simulations indicate that nanowire and core-shell nanowire battery geometries can potentially enable thin-film solid state batteries to overcome issues of inadequate energy and power per unit footprint. Cu nanotube core current collector and Ge sputtered shell can alleviate the volume expansion associated with high capacity anodes for lithium-ion batteries. Further work will be needed to investigate the cycle life over a large number of cycles and the rate capabilities of the anode.

ACKNOWLEDGMENTS

The authors would like to acknowledge the financial support from Science Foundation Ireland (SFI) Grant number: 12/IP/1722, Nanomaterials design and fabrication for energy storage and is supported in part by a research grant from SFI co-funded by the European Regional Development Fund under Grant Number 13/RC/2077.

REFERENCES

1. M. Doyle, T. F. Fuller and J. Newman, J. Electrochem. Soc. **140** (6), 1526 (1993).
2. V. Zadin, H. Kasemagi, A. Aabloo and D. Brandell, J. Power Sources **195** (18), 6218 (2010).
3. M. Hasan, T. Chowdhury and J. F. Rohan, J. Electrochem. Soc. **157** (6), A682 (2010).
4. J. Graetz, C. C. Ahn, R. Yazami and B. Fultz, J. Electrochem. Soc. **151** (5), A698 (2004).
5. D. Wang, Y.-L. Chang, Q. Wang, J. Cao, D. B. Farmer, R. G. Gordon and H. Dai, J. Am. Chem. Soc. **126** (37), 11602 (2004).
6. T. Kennedy, E. Mullane, H. Geaney, M. Osiak, C. O'Dwyer and K. M. Ryan, Nano Lett. **14** (2), 716 (2014).
7. M.-H. Park, Y. Cho, K. Kim, J. Kim, M. Liu and J. Cho, Angew. Chem. Int. Edit. **50** (41), 9647 (2011).
8. J. Wang, N. Du, H. Zhang, J. Yu and D. Yang, J. Mater. Chem. **22** (4), 1511 (2012).
9. T. Chowdhury, D. P. Casey and J. F. Rohan, Electrochem. Commun. **11** (6), 1203 (2009).
10. S. Barth, M. M. Koleśnik, K. Donegan, V. Krstić and J. D. Holmes, Chem. Mater **23** (14), 3335 (2011).
11. R. A. DiLeo, S. Frisco, M. J. Ganter, R. E. Rogers, R. P. Raffaelle and B. J. Landi, J. Phys. Chem. C **115** (45), 22609 (2011).
12. S. Fan, L. Y. Lim, Y. Y. Tay, S. S. Pramana, X. Rui, M. K. Samani, Q. Yan, B. K. Tay, M. F. Toney and H. H. Hng, J. Mater. Chem. A **1** (46), 14577 (2013)
13. V. Ho, W. Choi, C. Heng and V. Ng, Mater. Phys. Mech. **4**, 42 (2001).
14. P. K. Giri and S. Dhara, J. Nanomater. **2012** (2012).
15. B. Laforge, L. Levan-Jodin, R. Salot and A. Billard, J. Electrochem. Soc. **155** (2), A181 (2008).